Layout considerations on compound survival shelters for blast mitigation: A finite-element approach

Citation for published version:
Caçoilo, A, Mourão, R, Lecompte, D & Teixeira-Dias, F 2023, 'Layout considerations on compound survival shelters for blast mitigation: A finite-element approach', *International Journal of Protective Structures*, pp. 1-19. https://doi.org/10.1177/20414196231197701

Digital Object Identifier (DOI):
10.1177/20414196231197701

Link:
Link to publication record in Edinburgh Research Explorer

Document Version:
Peer reviewed version

Published In:
International Journal of Protective Structures

Layout considerations on compound survival shelters for blast mitigation: a finite-element approach

International Journal of Protective Structures
XX(X):2–20

DOI: 10.1177/ToBeAssigned
journals.sagepub.com/home/prs
SAGE

Andreia Caçoilo[1], Rodrigo Mourão[2], David Lecompte[3], Filipe Teixeira-Dias[4]

Abstract

The safety of both military personnel and equipment in unstable regions has for a long time been a major issue and concern. Protective shelters with multiple configurations have been widely used to meet safety requirements. Since military compounds are subjected to different types of threats, such as the detonation of improvised explosive devices (IED), a good understanding of the response of such shielding structures to blast waves is critical. A three-dimensional finite element (FE) model of a corner-entry ISO 20 ft container HESCO-Bastion survival shelter is developed, validated and tested under the external detonation of explosive charges. The FE model is validated against experimental data and used to investigate the protective performance of the shelter by considering several design-related parameters, such as charge location, roof extension, interior corridor dimensions, and the effect of venting and its location. Results are discussed in terms of peak overpressure and maximum impulse at discrete locations around the container, and it is found that the shelter is the least efficient in mitigating the blast load propagation when the explosive material is at an angle of $45°$ to the entrance. Also, while the protective roof at the entrance plays a significant role in protecting the container from air-borne threats, it is observed that it contributes to higher pressure and impulse data within the shelter, for detonations at ground level, with impulse amplifications as high as 94% when fully covering the entrance area. Contrarily, varying the distance between the container and the HESCO-Bastions is found to have minimal impact on the impulse, while naturally decreasing the peak pressure for increasing distances. Venting (through openings) can lead to up to 95% reduction in the peak pressure, whilst not affecting the impulse.

Keywords

Blast loading, survival shelter, HESCO-Bastion, finite element analysis, wave propagation

Introduction

Military operations in conflict regions are often at risk of being targeted by explosive threats, putting personnel and equipment safety under high risk. Soil-filled prefabricated galvanised steel weld-mesh units lined with non-woven polypropylene geotextile, such as the HESCO Bastion (HB) concertainers, have long been used by the military to build rapid field deployable blast walls to mitigate potential damage arising from such threats. Although these units can also be found in several civilian applications, their compactness and folding ability are most important for military expeditionary use, as this facilitates transportation prior to assembly (1).

The use of HB barrier walls to mitigate the effects of blast waves has been extensively investigated over the past years. Dirlewanger *et al.* (2) conducted an experimental program aiming to understand the structural response of HB walls under far-field explosive threats and expand the available data set to further improve modelling techniques. These authors identified the response mode to be tipping and sliding, and concluded that the overturning resistance of a HB barrier against blast loading is dependent on the moisture content of the base layer of contained soil. Scherbatiuk *et al.* (3) developed an analytical formulation that can be used to obtain the P-I diagram for a free-standing HB wall, with its rotation defined as the failure criteria. The authors showed that the required impulse to rotate the wall to 75% of the complete overturning angle and the required impulse to completely overturn the wall were very close. This indicates that the maximum rotation of the wall becomes increasingly sensitive to the impulse as the critical impulse required to completely overturn the wall is approached. Similarly, Scherbatiuk *et al.* (4) proposed an analytical model to calculate the vertical and horizontal displacement-time history responses of a free-standing soil-filled HB concertainer wall subjected to blast loading. Their model was developed based on experimental observations and delivers a

[1]Department of Mechanical Engineering, Stevens Institute of Technology, Hoboken, NJ, USA
[2]Stone Security Engineering, New York City, NY, USA
[3]Laboratory for Energetic Materials and Blasting Engineering, Royal Military Academy, Brussels, Belgium
[4]Institute for Infrastructure and Environment, School of Engineering, The University of Edinburgh, Edinburgh EH9 3FG, UK

Corresponding author:
Andreia Caçoilo, Department of Mechanical Engineering, Stevens Institute of Technology, Hoboken, NJ, USA
Email: acacoilo@stevens.edu

good agreement with experimental data, for the early time histories, specially before the wall overturns, from when additional mechanisms come into play.

These studies have primarily been focused on the structural response of HB walls to blast loading and, to date, the attenuation effects on blast waves attributed to the HB have been minimally investigated, particularly for large TNT-equivalent explosions. The exception may be the work of Xu *et al.* (5), who conducted one of the few experimental test series on HB barriers aiming to record the overpressure at key locations around the HB wall. Their findings indicate that peak overpressure is minimally affected by the blast wall thickness, whereas the height of the wall and proximity of the measurement location to the back face are the controlling parameters for the blast wave attenuation, allowing for the derivation of an empirical formulation for the back wall overpressure of a HB.

In addition to general defensive barriers, HB units are typically used to form protective structures, where units are stacked or placed adjacent to each other, fully encapsulating sensitive equipment or creating safe areas for personnel. Smaller units can also be used to form roof covers, provided beam-like supporting elements and decking sheets are also used. Examples of such structures are generic protective shelter compounds, where standard ISO 20 ft shipping containers are confined by HB units. Such structures, however, may induce high levels of confinement and increase the magnitude of the blast waves propagating in its interior, due to multiple reflections and spurious effects.

Although confined explosions have been studied in different settings, such as urban environments (6; 7; 8; 9; 10), tunnels (11; 12; 13) and small-size closed compartments and rooms (8; 14; 15; 16; 17), where the flow of blast waves is constrained by obstacles and non-straight narrow paths, very limited research on blast wave propagation within survival shelters is available. In one of the few available studies, Lecompte *et al.* (18) conducted a series of experimental blast tests on a laboratory-scale survival shelter using a modular building system (e.g., commercially available plastic building blocks). These authors aimed to record internal pressure and impulse data using different shelter layouts — corner-entry and flow through — and developed a finite element (FE) model of the system. Although the authors identified the detachment of the inter-brick connections as a limitation of their small-scale model, results were still considered acceptable and their approach a reasonably quick tool to obtain preliminary estimates of the magnitude of the blast wave propagating within the protective shelter. Aiming to improve this methodology and to conduct a thorough study on the blast wave propagation within protective shelters, Caçoilo *et al.* (19) developed a 1:10 scale model of a corner-entry survival shelter made of steel protected wood panels. Contrarily to the model presented by Lecompte *et al.* (18), this improved version was developed so that the assumption of rigid walls remain valid and pressure data could be accurately measured. The authors also developed a three-dimensional finite element model of the experimental set-up that was used to assess the blast propagation within the shelter over time, rather than just obtaining pressure and impulse data at discrete locations.

It is clear from the studies presented above that shock waves propagate in confined spaces, such as protective shelters, in complex ways, as a multitude of reflections, diffractions, and superpositions can occur, resulting in atypical pressure measurements and unexpected structural responses. Over the last two decades, several studies have examined the influence of load shape on structural response of systems. In the work of Huang *et al.* (20), the effect of pulse shape on underground structures subjected to internal blast loads was studied, indicating that pulse shape was critical in the damage analysis of buried structures. Tan *et al.* (21) conducted a numerical study to evaluate pulse shape effects on the ultimate blast capacity of steel beams. It was found that their blast resistance gradually decreased with exponential, triangular, and rectangular loading profiles. Moreover, Sauvan *et al.* (**?** , sauvan2012)erformed an experimental study to evaluate the variation of blast parameters in confined spaces, including overpressure, impulse, and arrival time, by progressively increasing the confinement level of the testing setting. According to the authors, in semi-confined environments, damage levels caused by the negative phase of the blast wave can be greater than the damage caused by the positive phase alone. In a similar study, Kang *et al.* (22) have found that negative pressures should be included in blast analyses to obtain accurate structural responses. More recently, Cacoilo *et al.* (23) presented an extensive numerical work on evaluating the influence of several wave-related parameters on the structural response of corrugated metal plates, i.e. impulse trains, complex pressure profiles, and signal simplifications. The authors reported that correctly defining the negative impulse train in the pressure-time history is one of the main factors leading to accurate modelling of the mechanical response of the structure, highlighting the need to fully understand the effects of confinement on pressure measurements.

HESCO-based protective shelters are highly flexible in design, allowing separate modules to be attached in a number of different layouts. Such layout modifications can lead to major implications with regards to the load acting on the container, which can drastically influence its structural performance and, consequently, the safety of its occupants. Such design adjustments, sometimes introduced due to operational constraints in remote field operations, require designers and engineers to make informed decisions. Within the above framework, this paper proposes a finite element model of a standard ISO 20 ft steel container survival shelter subjected to the detonation of explosive charges. The model is validated against experimental data and used to investigate the influence of the shelter design on the overall blast wave propagation, maximum overpressure and specific impulse, considering different design-related parameters, such as charge location, roof extension, interior corridor dimensions, and the effect of venting and its location.

Experimental results

Caçoilo *et al.* (19) presented a laboratory-scale experimental study on the blast wave propagation inside a HESCO-Bastion compound (HBC) survival shelter. The authors conducted a series of blast tests with explosive charges located at 0.5 and 1 m from the entrance, with an angle of incidence of 45°. The test set-up, shown in Figure 1, was scaled down with a reduction factor $\lambda = 10$ and entirely built out of plywood. It features the representative HESCO wall barriers and container, as well as the ground and protective roof. To represent a hemispherical explosion, typical from those occurring from the detonation of air-borne threats after reaching the ground, the explosive charges were placed at the entrance of the compound model and in contact with the structure's ground. Foam was used to hold the explosive charges and detonator in place (see Figure 1(c)). Although the experimental tests were conducted with a fixed mass of explosive, part of the blast wave propagated through the opening where the foam was inserted, reducing the intensity of the effective blast wave impinging the HBC. The energy fraction that is lost underneath the base plate was identified based on external pressure measurements coupled with the Kingery-Bulmash empirical equations. The blast pressure acting on the structure is estimated to be equivalent to 3.3 g of TNT. The blast wave propagation within the HBC was monitored through the use of pressure transducers fixed to each face of the container. A full description of the experimental details can be found in Caçoilo *et al.* (19).

Numerical framework

Model description

The numerical framework presented in this paper was developed using the commercially available general-purpose finite element code LS-DYNA. An overall view of the model developed to describe the small-scale experimental work is shown in Figure 2. The air domain inside the shelter was discretised with reduced integration eight-node hexahedral elements using an ALE formulation. The model is based on a coupled framework, combining the Multi-Material Arbitrary Lagrangian-Eulerian (MM-ALE) and the Load Blast Enhanced approaches (24). The coupling method avoids modelling the high-explosive and its detonation explicitly by allowing a pressure-time history to be applied on a single layer of elements of the ALE mesh instead, based on the Kingery-Bulmash empirical equations (25). This is referred to as the *ambient layer*, which

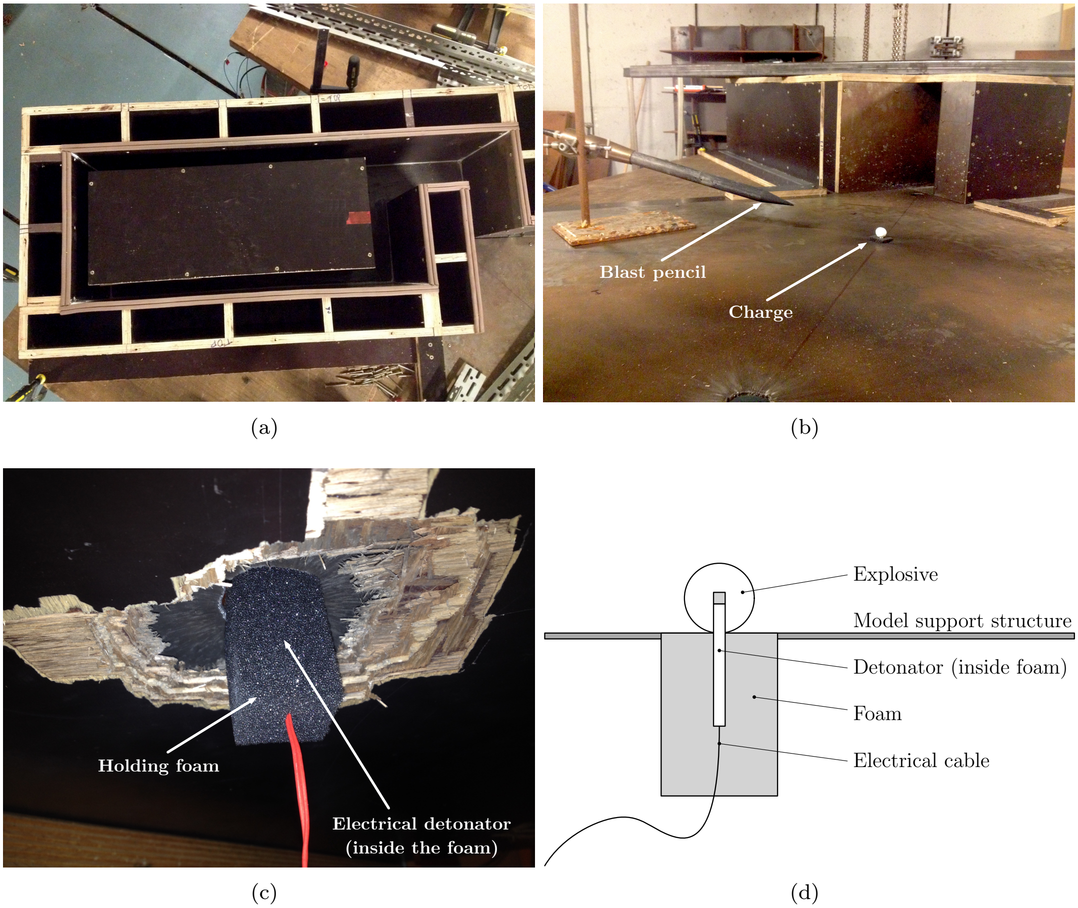

Figure 1. Experimental set-up: (a) top view (with roof removed); (b) overall view; (c) detonator holding system; and (d) schematics of the high explosive support system. Reprinted with permission of Springer Nature, from Caçoilo *et al.* (19); permission conveyed through Copyright Clearance Center.

makes the exterior surface of the air domain act as a receptor of the blast wave parameters and convert them into thermodynamic state data, which are subsequently applied as a source onto the adjoining ALE finite elements (26). The assumption of rigid shelter and container surfaces was modelled by restraining the boundary nodes of the air domain to behave as fully reflective surfaces. While this is expected to lead to a slight overestimation of pressure and impulse, it is not expected to influence the wave reflection profile along the confined space. Pressure data is obtained by setting a number of tracer points — the numerical equivalent to pressure gauges — at

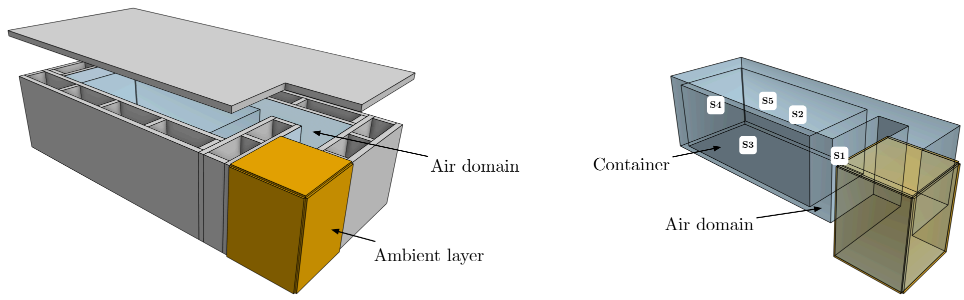

(a) (b)

Figure 2. HESCO-Bastion compound (HBC) survival shelter: (a) overall view of 3D model with air domain (shown in blue); and (b) wireframe view of ISO container and pressure tracer locations: S1 - front face, S2 - right face, S3 - left face, S4 - back face and S5 - top face. While the specific charge location depends on the analysis conducted, it typically faces the entrance corner (adapted from Cacoilo *et al.* (19)).

the centre of all five faces of the container, coinciding with the locations where the pressure data was experimentally recorded. While additional locations on each face of the container could have been used to predict pressure data, Cacoilo *et al.* (27) demonstrated that very little variation in pressure data across multiple locations on each face of the container is observed. Consequently, only the centre of each face (S1, S2, S3, S4 and S5) were used for pressure measurements in this study. Spurious zero energy (hourglass) modes, typical of under-integrated formulations (28; 29), are controlled with a viscous hourglass algorithm. This approach is in line with research that suggests the viscous form to be more suitable for high-strain rate events, such as blast and shock waves, than the stiffness form (30; 31).

Material modelling

The air domain is widely considered an ideal gas for the study of several aerodynamic problems, satisfying the ideal gas law (32). As such, the material type `MAT_NULL` is used to define the evolution of the density of air, while the pressure is defined by a linear-polynomial equation of state, given by

$$P = C_0 + C_1\mu + C_2\mu^2 + C_3\mu^3 + \left(C_4 + C_5\mu + C_6\mu^2\right) E, \tag{1}$$

where C_i (with $i = 0, \ldots, 6$) are material constants, E is the specific internal energy and μ is the compression factor

$$\mu = \frac{\rho}{\rho_0} - 1, \tag{2}$$

where ρ/ρ_0 is the ratio of the current density to the reference density. For an ideal gas, such as air, the linear-polynomial in equation 1 can be reduced to

$$P = (\gamma - 1)\,\frac{\rho}{\rho_0} E_0, \tag{3}$$

with $\gamma = 1.4$ for small overpressures (33). This reduction is achieved by setting $C_0 = C_1 = C_2 = C_3 = C_6 = 0$ and $C_4 = C_5 = \gamma - 1$, where γ is the ratio of specific heat at constant pressure and volume ($\gamma = c_\mathrm{p}/c_\mathrm{v}$). All material properties are listed in Table 1.

Table 1. Material and equation of state properties and constants for air (34).

Material	Parameter	Value
Air	Density, ρ	1.225 kg/m^3
	$C_0 = C_1 = C_2 = C_3 = C_6$	0
	$C_4 = C_5$	0.4
	Specific internal energy, E	2.5×10^{-4} kJ/kg

Conservation of mass, momentum and internal energy in the advection process is enforced with the van Leer and Half-Index-Shift formulation (35), which is known to accurately capture overpressure peaks and is recommended when detonation products are omitted (19). Advection methods are described in detail by Young (36) and Benson (37).

Model validation

The ability of the proposed FE model to accurately replicate and predict pressure and impulse data is verified against experimental results by Caçoilo *et al.* (19). The model was used to replicate the test conducted by these authors at a distance of 1 m from the entrance, and an angle of incidence of 45°. Figure 3 shows a comparison between the predicted and experimental pressure and specific impulse time-histories, measured at the centre of each face of the container, as outlined in Figure 2(b).

Overall, pressure data is well captured by the numerical model, more critically the first positive overpressure peak. Although the numerical model slightly overpredicts pressure data after the first positive peak (leading to an overprediction on cumulative impulse), most probably due the assumption of rigid boundary conditions, it is able to accurately predict the overall pressure trend and localised reflection induced peaks on all faces of the container.

Overall, relative errors of the computed maximum overpressure range from 0.2 to 29.8%, while differences in specific impulses range from 4.7 to 48.9%. Although differences in the specific

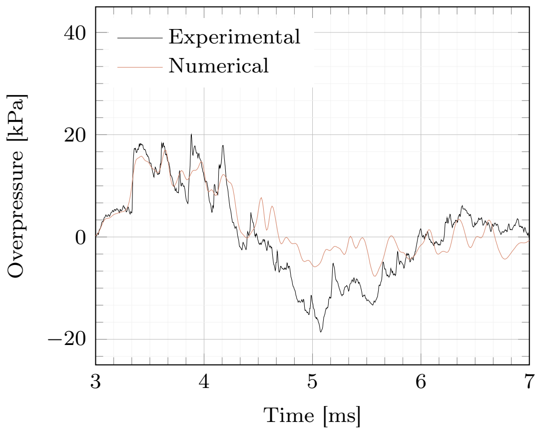
Experimental
Numerical
Overpressure [kPa]
Time [ms]
40
20
0
−20
3
4
5
6
7

(a)

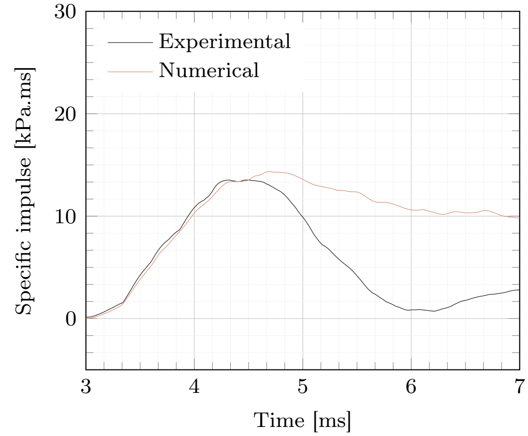
Experimental
Numerical
Specific impulse [kPa.ms]
Time [ms]
30
20
10
0
3
4
5
6
7

(b)

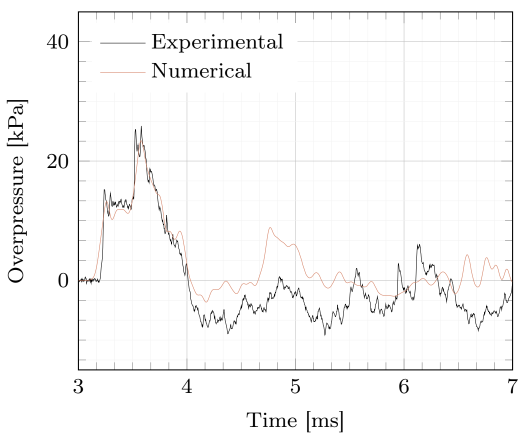
Experimental
Numerical
Overpressure [kPa]
Time [ms]
40
20
0
3
4
5
6
7

(c)

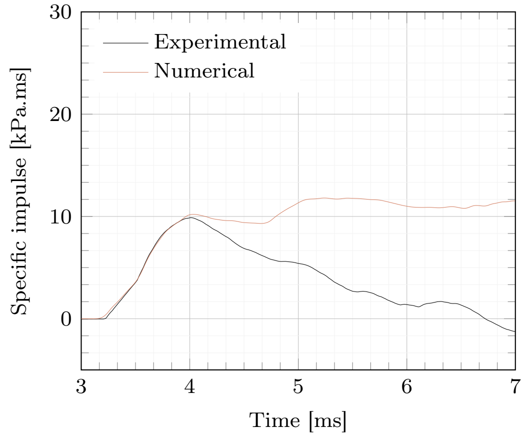
Experimental
Numerical
Specific impulse [kPa.ms]
Time [ms]
30
20
10
0
3
4
5
6
7

(d)

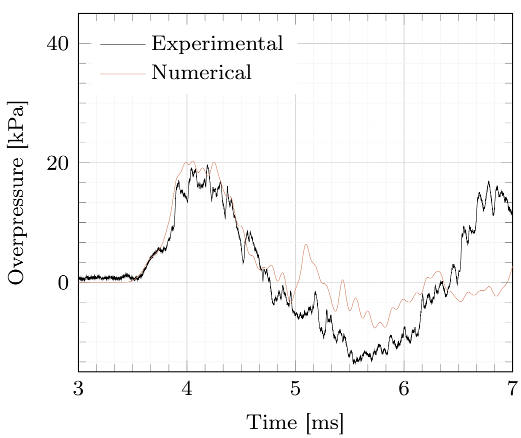
Experimental
Numerical
Overpressure [kPa]
Time [ms]
40
20
0
3
4
5
6
7

(e)

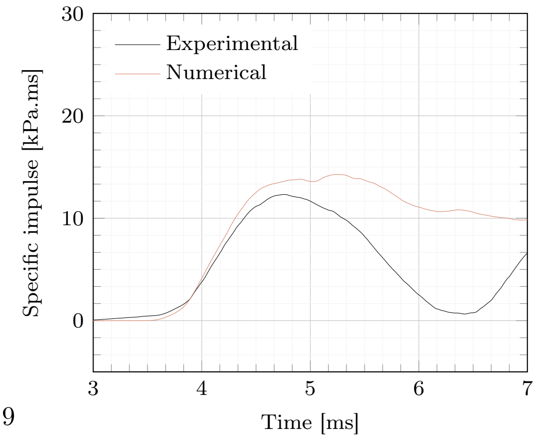
Experimental
Numerical
Specific impulse [kPa.ms]
Time [ms]
30
20
10
0
3
4
5
6
7

(f)

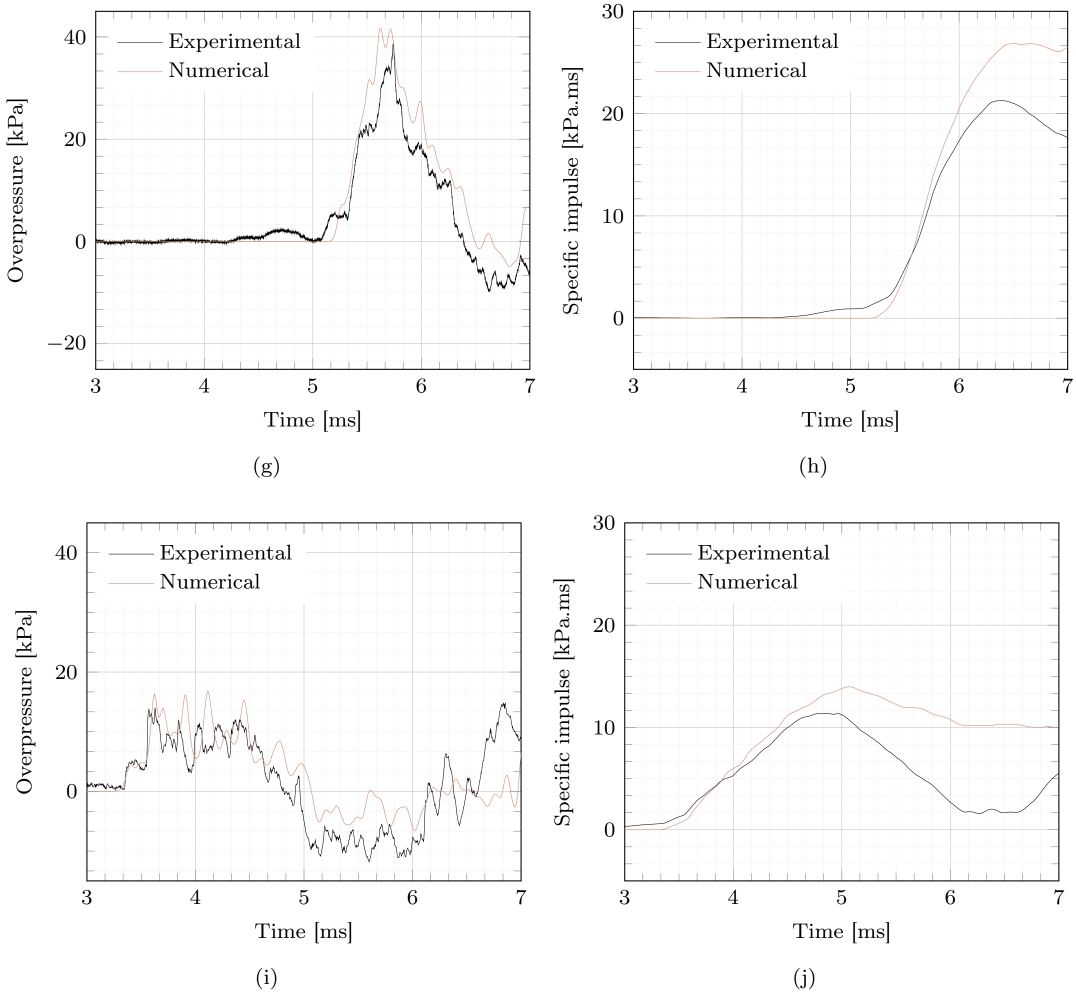

Figure 3. Comparison between numerical and experimental overpressure and impulse time-histories, for a charge located at 1 m from the entrance, at an angle of $45°$: (a-b) sensor S1, (c-d) sensor S2, (e-f) sensor S3, (g-h) sensor S4 and (i-j) sensor S5.

impulse are bigger than those for pressure, they can be explained by the cumulative nature of the specific impulse, which is amplified by a continuous overestimation of pressure. Overall, such results indicate a good match with the experimental results, highlighting the strength of the proposed model and the corresponding numerical predictions.

Results and discussion

This section presents the results of the analyses that were done with the developed model, regarding operational aspects of the construction and position of the HBC within military expedition compounds. This is highly relevant as such factors play a key role in minimising the loads acting on the interior container. Conditions used for validating the FE model (i.e. explosive charge located at 1 m from the entrance, at an angle of incidence of 45° relative to the entrance) will be used as a baseline for further studies.

Charge location

The entrance of the shelter naturally represents its most vulnerable location when considering the detonation of a high-explosive (HE) charge. It is nonetheless important to determine the most critical angle with respect to the survival shelter's entrance. Three different positions of the charge were considered, with increasing angles angles of incidence: 0°, 45° and 90° between the entrance axis and the location (position vector) of the HE charge, as shown in Figure 4.

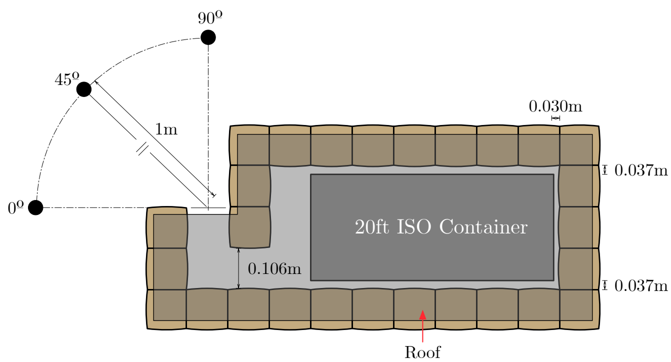

Figure 4. Top view of the shelter and locations of the charge for the reference layout (adapted from Cacoilo *et al.* (19)).

Figures 5(a) and 5(b) show that a charge located at 45° yields the highest values of peak overpressure and specific impulses on the different faces of the container. Although the minimum overpressure is recorded for an angle of 0°, differences to an angle of 90° are minimal, with an overpressure variation ranging from 1.2 to 5.7 kPa, for sensors S2 and S1, respectively. A similar trend is observed for specific impulses, where such variation ranges from 2.9 to 3.6 kPa.ms, for sensors S3 and S4, respectively. The maximum overpressure and specific impulse differences were observed for sensor S4, corresponding to 12.5 kPa and 10.3 kPa.ms, respectively.

Overall, significant sensitivity on the results with respect to the charge location is observed, with a maximum difference of 42% and 80% for maximum overpressure and specific impulse, respectively.

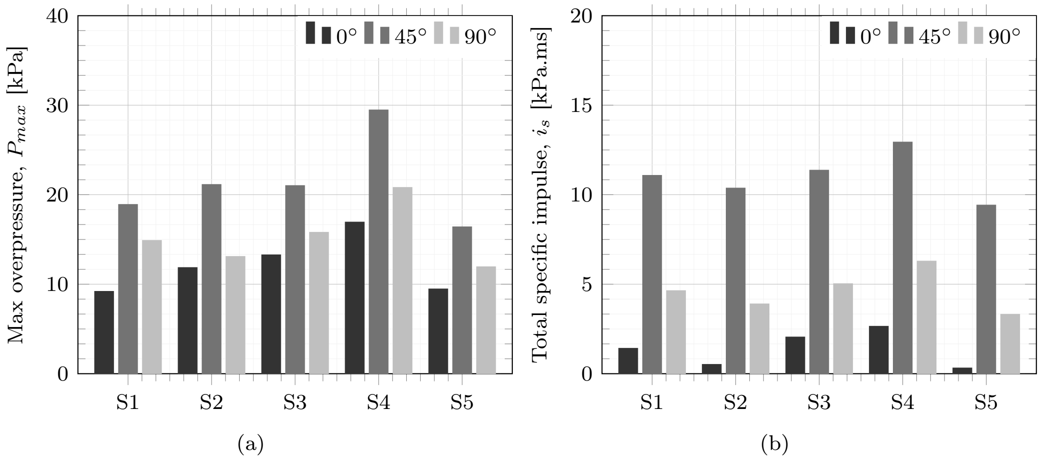

Figure 5. Comparison of (a) maximum overpressure and (b) specific impulse for different charge locations.

Protective roof

Protection against direct air-borne threats, such as mortars, can be efficiently achieved by increasing the extension of the protective roof, which is a key element in providing additional stand-off distance. The propagation of the blast wave within the shelter may, however, result in higher pressures and loads on the container due to the consequent increased confinement level. The influence of such geometric considerations is assessed by considering three different layouts for the protective roof: Ref (typical entrance); R2 (non-protected entrance) and R3 (fully protected entrance). Schematic representations of the different layouts are shown in Figures 6(a) to 6(c). The analysis is conducted with explosive charges located at 0°, 45° and 90°, for a constant stand-off distance of 1 m.

The most critical charge location for the three roof layouts corresponds to a 45° angle, as shown by the results in Figure 7. Layout R2, when compared to the reference layout, delivers a general decrease in peak overpressure and specific impulse. Reductions of 15% and 100% are achieved for peak overpressure and specific impulse, respectively, as listed in Table 2. Nevertheless, when comparing layout R3 to the reference layout, the maximum relative differences are 21% for overpressure and 94% for specific impulse. This is generally explained by the increased

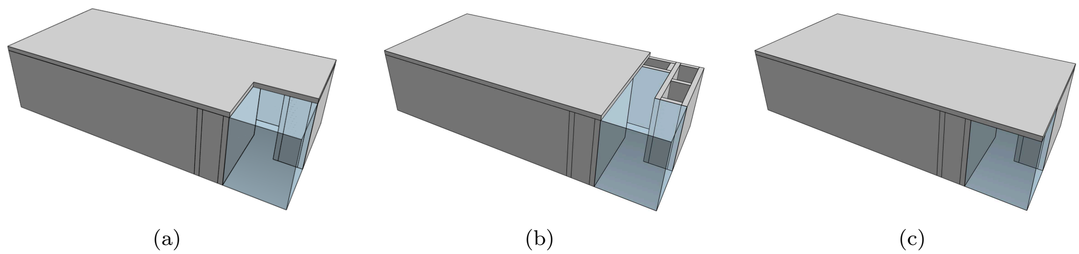

Figure 6. Geometric considerations for the protective roof: (a) Reference, (b) R2 and (c) R3.

Table 2. Relative differences on the maximum overpressure and specific impulse for the different layouts of the protective roof, comparing with the reference layout for sensor S4, where (+) indicates an increase and (−) a decrease of the absolute value of maximum overpressure and specific impulse.

Charge location	R2		R3	
	ΔP_{max} (%)	Δi_{s} (%)	ΔP_{max} (%)	Δi_{s} (%)
0°	−15	−100	+19	+94
45°	−13	−28	+21	+47
90°	−14	−49	+15	+66

confinement level provided by layout R3. While layout R2 allows the blast wave to propagate upwards and escape the shelter, reducing the intensity of the blast wave in the inner area, layout R3 provides additional blast wave superposition due to the added roofing area. As such, layout R2 proves to be more efficient in protecting the container from the detonation of charges located in close proximity to the entrance. This layout, however, increases the risk of air-borne threats detonating in the non-protected entrance corridor, which may result in significantly higher loads acting on the container due to the reduced stand-off distance.

Corridor dimensions

Due to the highly modular nature of HB construction, the gap between the ISO container and the HB walls, typically referred to as internal corridors, can be easily set-up and modified on site to fulfil operational needs. Similar to the propagation of blast waves in urban scenarios, where different path widths result in significantly different peak pressure and impulse (38), varying the gap widths in a survival shelter may considerably affect its protective performance, by amplifying/reducing the load acting on the steel container. The influence of different gap widths on the blast wave propagation is thus evaluated by considering three different layouts. Results are compared against the reference layout, with the charge facing the entrance at 45°, as shown in Figure 8(a). Layouts C1 and C2 provide wider lateral and rear corridors, respectively, as shown in Figures 8(b) and 8(c). Layout C3 provides the combined geometry of layouts C1 and C2 (see Figure 8(d)).

Overpressure and specific impulse data is shown in Figures 9(a) and 9(b), respectively. As expected, layouts C1 and C3, with enlarged lateral corridors, attenuate the maximum overpressure recorded in all sensors, when compared to the reference layout. This reduction is, however, more evident for sensor S3, where the maximum overpressure is approximately 62% lower than the reference layout. Additionally, peak overpressure in sensors S1 and S5 is observed to have the smallest decrease, at 11 and 9%, respectively. This might be explained by the fact that those sensors (front and top) are located in regions that have the same gap as the reference layout. Considering layout C2, it is clear that by independently increasing the gap at the rear of the compound only affects the peak overpressure recorded in sensor S4, located in that same region.

Figure 9(b) shows very little differences in the specific impulse recorded for layouts C1, C2 or C3, relative to the reference layout, with differences ranging from 0.1% to 17%, for sensors S3 and S4, respectively. From this set of results, it is clear that none of the proposed layouts deliver a consistent impulse decrease in all sensors, contrarily to what happens in terms of peak overpressure. According to previous research on the response of corrugated plates under blast loading, the structural response under dynamic loading is dominated by the specific impulse (23). The minimal impulse variations observed across the different layouts translates into minimal variation of the ISO container response when considering the different gap widths between the container and HB walls. Although such geometry modifications might not show a clear advantage from a performance point of view, they can be considered from an operational perspective, as the protective capacity of the shelter is not compromised.

Effects of venting

Previous results indicate that the rear of the container is in most cases the face subjected to higher loads, mostly due to the superposition of shock waves travelling on both sides of the container. As such, the effect of including openings in the vicinity of this location, intending to reduce the maximum overpressure, should be analysed. Figure 10 shows the venting locations addressed in this study. All venting conditions are based on the reference layout, with the HE charge located at 45° with respect to the entrance and a stand-off distance of 1 m.

Maximum overpressure and specific impulse for the different venting configurations are shown in Figures 11(a) and 11(b). As should be expected, only sensor S4 presents variations in the calculated maximum overpressure, as the shock front propagates similarly through the lateral corridors when compared to the absence of venting. While this is true for the maximum overpressure, as it is typically obtained in the first passage of the wave, the total specific impulse, however, varies from the reference case for all sensors. This is due to the fact that after reaching the opening, the blast wave propagates backwards with a new set of reflections and superpositions, leading to a different pressure-time history and, consequently, a different total specific impulse. Comparing to the absence of venting openings, a reduction of 14% on maximum overpressure in sensor S4 is observed for layouts BO and LO, while layout RO leads to a decrease of approximately 35%. With a general decrease of the maximum specific impulse for all venting options, significant reductions of about 95%, 94% and 86% are observed for layouts BO, LO and RO, respectively.

Entrance confinement

The effectiveness of alternative entrance layouts in attenuating the intensity of the shock wave propagating within the HB shelter is evaluated with two different layouts with additional entrance barriers and one layout with a simplified entrance, as shown in Figure 12. It aims to understand how an increased stand-off distance provided by longer entrance corridors compares with smaller and less confined entrance areas. All layouts are evaluated with a charge located at 1 m from the entrance and increasing angles of incidence. Results are compared against the reference layout (see Figure 4).

On the one hand, it is clear that different confinement levels at the entrance of the shelter have minimal effect on the peak overpressure, as shown by the results in Figure 13. On the other hand, the specific impulse is found to be highly sensitive, with a maximum difference of nearly 72%, for a charge positioned at 45°, across the different layouts.

Charges located at 45°, as shown in Figures 13(a) and 13(b), are found to induce the higher impulse variations across the different layouts. While the long entrance corridors of layouts E1 and E2 play a key role in increasing the impulse recorded in all sensors, when compared to the reference layout, the low confinement and reduced channelling effects at the entrance of layoput E3 leads to a generalised decrease of the impulse for all sensors. Overall, layouts E1 and E2 drive a maximum increase in the impulse of 56% and 211%, respectively, while layout E3 is able to reduce the impulse recorded in the reference layout by a maximum of 43%.

Charges located in the vicinity of the shelter entrance with an angle of incidence of 0° induce the lowest peak overpressure and impulse across all different layouts, as demonstrated by the results in Figure 13(c) and 13(d). This can be explained by the fact that the charge is not facing the entrance directly, which contributes to reducing the amount of energy actively entering the shelter. Specifically, layout E3 is the one to offer best performance in reducing the maximum impulse, as most sensors register negative maximum impulses values. This is a good indicator of better structural performance under both dynamic and impulsive regimes, when compared with a positive maximum impulse (23).

Considering the charge located at an angle of 90°, while the maximum impulse recorded in layout E1, E2 and E3 is similarly across all sensors, the reference layout leads to lower maximum impulse, with differences ranging from 40% to 77% for sensors S1 and S3, respectively. Layout E3, however, shows the highest differences in peak overpressure, specifically in the front (sensor S1), rear (sensor S4) and top (sensor S5) faces, when compared to the remaining layouts, which present very similar peak overpressure. These observations can be explained by the fact that the detonation of a charge at 90° occurs directly in front of the entrance of Layout E3, which results in a higher intensity shock wave around the container.

Concluding remarks

This paper presents a comprehensive study on the protective performance of an ISO 20ft steel container HESCO-Bastion survival shelter subjected to the exterior detonation of explosive charges, aiming to provide design recommendations at the shelter level, for a better protection of military personnel in operational conditions. A three-dimensional finite element model is developed and validated against experimental data and used to investigate the influence of key design and construction parameters to which designers and engineers may need to pay special attention. These parameters include the location of the high-explosive charge, the extension/configuration of the protective roof, the dimension of the gap between the HESCO-Bastion barriers and the ISO container, the effect of venting and the entrance confinement. While this study focuses on peak overpressure and maximum impulse, rather than the structural response of the container, the significance of the findings is discussed throughout the paper. From the obtained results it can be concluded that:

- While it is difficult to estimate the magnitude of blast waves propagating through complex environments, such as the interior of a ISO container survival shelter, using conventional analytical methods, three-dimensional FE modelling has been proven to be a valuable tool for investigating such scenarios. Additionally, the proposed FE model of the survival shelter is found to deliver accurate results when compared to experimental data.

- The exact location of the high-explosive charge plays a critical role on the peak overpressure and impulse recorded at the faces of the container, with an angle of incidence of 45° leading to the highest overpressure and impulse.
- The configuration and extension of the protective roof over the entrance of the shelter is a major design parameter when the maximum impulse is considered. The absence of a roof over the entrance can lead to a maximum impulse reduction of nearly of 100%, compared to a configuration with 50% of the entrance covered. Contrarily, fully covering the entrance increases the maximum impulse to by approximately 94%.
- An increased gap between the HESCO-Bastion walls and the container is found to have minimal influence on the maximum impulse. It is, however, observed that it can lead to reduced peak overpressure, most critically at the enlarged corridors.
- The inclusion of venting on the shelter, specifically at the rear, where the propagating shock waves meet and superimpose, has minimal influence on the peak overpressure. Nonetheless, it has a major impact on the maximum impulse, with reductions of up to 95% when comparing to the shelter layout with no openings.
- Increasing the confinement level of the entrance by extending the entrance corridors typically induces higher maximum impulses but no significant variation of the peak overpressure. It should be noted that by removing the entrance corridor and having a direct entrance to the shelter can actively mitigate the maximum impulse observed in the container, the exception being the case where the charge is located directly in front of the entrance.
- Although some of the investigated layouts might not have a clear advantage from a protection performance point of view, they may be considered from an operational perspective. While the magnitude of the blast wave propagating within the shelter might be of great concern, design modifications can also lead to vulnerable situations where the container might end up being exposed to other direct threats. As such, the presented findings should be used with active judgement, considering the particularities of the scenario and the full threat vector to which the shelter might be exposed to.

Declaration of conflicting interests

The Authors declare that there is no conflict of interest.

References

[1] Smith P. Blast walls for structural protection against high explosive threats: A review. *International Journal of Protective Structures* 2010; 1(1): 67–84. DOI:10.1260/2041-4196.1.1.67.

[2] Dirlewanger H, Pope D, Russel D et al. Enhancement of hesco bastion wall models to better predict magnitudes of response under far-field loading conditions. In *17th International Symposium on the Interaction of the Effects of Munitions with Structures*. Germany.

[3] Scherbatiuk K, Rattanawangcharoen N, Pope D et al. Generation of a pressure–impulse diagram for a temporary soil wall using an analytical rigid-body rotation model. *International Journal of Impact Engineering* 2008; 35(6): 530–539. DOI:https://doi.org/10.1016/j.ijimpeng.2007.04.006.

[4] Scherbatiuk K and Rattanawangcharoen N. A hybrid rigid body rotation model for predicting a response of a temporary soil-filled wall subjected to blast loading. *International Journal of Impact Engineering* 2010; 37(1): 11–26. DOI:https://doi.org/10.1016/j.ijimpeng.2009.06.014.

[5] Xu R, Chen L, Fang Q et al. Protective effects of gabion wall against blast waves from large tnt-equivalent explosions. *Engineering Structures* 2021; 249: 113389. DOI:https://doi.org/10.1016/j.engstruct.2021.113389.

[6] Kinney G and Graham K. *Explosive Shocks in Air*. 2nd edition ed. New York: Springer, 1985. ISBN 978-3-642-86682-1.

[7] Baker W, Cox P, Westine P et al. *Explosion Hazards and Evaluation*. Fundamental Studies in Engineering, Amsterdam: Elsevier Science B. V., 1983. ISBN 978-0-444-42094-7.

[8] Julien B, Sochet I and Vaillant T. Impact of the volume of rooms on shock wave propagation within a multi-chamber system. *Shock Waves* 2016; 26: 87–108. DOI:10.1007/s00193-015-0603-2.

[9] Smith P, Whalen G, Feng L et al. Blast loading on buildings from explosions in city streets. In *Proceedings of the Institution of Civil Engineers Structures & Buildings*, volume 146. pp. 47–55. DOI:10.1680/stbu.2001.146.1.47.

[10] Fouchier C, Laboureur D, Youinou L et al. Experimental investigation of blast wave propagation in an urban environment. *Journal of Loss Prevention in the Process Industries* 2017; 49: 248–265. DOI:10.1016/j.jlp.2017.06.021.

[11] Skews B and Law W. The propagation of shock waves in a complex tunnel system. *Journal of the Southern African Institute of Mining and Metallurgy* 1991; 91: 137–144.

[12] Smith P, Mays G, Rose T et al. Small scale models of complex geometry for blast overpressure assessment. *International Journal of Impact Engineering* 1992; 12: 345–360. DOI:10.1016/0734-743X(92)90112-7.

[13] Rigas F and Sklavounos S. Experimentally validated 3-D simulation of shock waves generated by dense explosives in confined complex geometries. *Journal of Hazardous Materials* 2005; 121: 23–30. DOI:10.1016/j.jhazmat.2005.01.031.

[14] Anthistle T, Fletcher D and Tyas A. Characterisation of blast loading in complex, confined geometries using quarter symmetry experimental methods. *Shock Waves* 2016; 26: 749–757. DOI: 10.1007/s00193-016-0621-8.

[15] Geretto C, Chung Kim Yuen S and Nurick G. An experimental study of the effects of degrees of confinement on the response of square mild steel plates subjected to blast loading. *International Journal of Impact Engineering* 2015; 79: 32–44. DOI:10.1016/j.ijimpeng.2014.08.002.

[16] Salvado F, Tavares A, Teixeira-Dias F et al. Confined explosions: The effect of compartment geometry. *Journal of Loss Prevention in the Process Industries* 2017; 48: 126–144. DOI: 10.1016/j.jlp.2017.04.013.

[17] Sauvan P, Sochet I and Trélat S. Analysis of reflected blast wave pressure profiles in a confined room. *Shock Waves* 2012; 22: 253–264. DOI:10.1007/s00193-012-0363-1.

[18] Lecompte D, De Schepper R, Belkassem B et al. A modular building-block system for lab-scale explosive testing of urban type configurations. In *23rd Military Aspects of Blast and Shock*. Oxford, p. 16.

[19] Caçoilo A, Teixeira-Dias F, Mourão R et al. Blast wave propagation in survival shelters: Experimental analysis and numerical modelling. *Shock Waves* 2018; 28(6): 1169–1183. DOI: 10.1007/s00193-018-0858-5.

[20] Huang X, He L and Ma GW. Soil-structure interaction and pulse shape effect on structural element damage to blast load. *Journal of Performance of Constructed Facilities* 2011; 25(5): 400–410. DOI: 10.1061/(ASCE)CF.1943-5509.0000229.

[21] Tan Y, Xi F, Li S et al. Pulse shape effects on the dynamic response of a steel beam under combined action of fire and explosion loads. *Journal of Constructional Steel Research* 2017; 139: 484–492. DOI:10.1016/j.jcsr.2017.10.001.

[22] Kang KY, Choi KH, Choi JW et al. An influence of gas explosions on dynamic responses of a single degree of freedom model. *Shock and Vibration* 2016; 2016: 1–13. DOI:10.1155/2016/9582702.

[23] Caçoilo A, Mourão R, Teixeira-Dias F et al. Structural response of corrugated plates under blast loading: The influence of the pressure-time history. *Structures* 2021; 30: 531–545. DOI: 10.1016/j.istruc.2021.01.025.

[24] Slavik T. A coupling of empirical explosive blast loads to ALE air domains in LS-DYNA. *IOP Conference Series: Materials Science and Engineering* 2010; 10. DOI:10.1088/1757-899X/10/1/012146.

[25] Kingery C and Bulmash G. Air- blast parameters from TNT spherical air burst and hemispherical surface burst. Technical Report ARBRL (TR-02555), Ballistic Research Laboratory, Maryland, 1984.

[26] Shuaib M and Daoud O. Numerical analysis of RC slab under blast loads using the coupling of LBE and ALE method in LS-DYNA. In *Fib Symposium*. Cape Town.

[27] Caçoilo A, Mourão, Belkassem B et al. Blast wave assessment in a compound survival container: Small-scale testing. *Proceedings* 2018; 2(8). DOI:10.3390/ICEM18-05459.

[28] Consolazio G, Chung J and Gurley K. Impact simulation and full scale crash testing of a low profile concrete work zone barrier. *Computers & Structures* 2003; 81: 1359–1374. DOI: 10.1016/S0045-7949(03)00058-0.

[29] LSTC. LS-DYNA Theory manual, 2006.

[30] Alia A and Souli M. High explosive simulation using multi-material formulations. *Applied Thermal Engineering* 2006; 26: 1032–1042. DOI:10.1016/j.applthermaleng.2005.10.018.

[31] Flanagan D and Belytschko T. A uniform strain hexahedron and quadrilateral with orthogonal hourglass control. *International Journal for Numerical Methods in Engineering* 1981; 17: 679–706. DOI:10.1002/nme.1620170504.

[32] Vallerani E. An "ideal equivalent gas method" for the study of shock waves in supersonic real gas flows. *Meccanica* 1969; 4(3): 234–249. DOI:10.1007/BF02133438.

[33] Dobrociński S and Flis L. Numerical simulations of blast loads from near-field ground explosions in air. *Studia Geotechnica et Mechanica* 2015; 37(4): 11–18. DOI:10.1515/sgem-2015-0040.

[34] Ousji H, Belkassem B, Louar M et al. Parametric study of an explosive-driven shock tube as blast loading tool. *Experimental Techniques* 2016; 40: 1307–1325. DOI:10.1111/ext.12179.

[35] Van Leer B. Towards the ultimate conservative difference scheme. IV. A new approach to numerical convection. *Journal of Computational Physics* 1977; 23: 276–299. DOI:10.1016/0021-9991(77) 90095-X.

[36] Youngs D. Time-dependent multi-material flow with large fluid distortion. *Numerical Methods for Fluid Dynamics* 1982; 24: 273–285.

[37] Benson D. Momentum advection on a staggered mesh. *Journal of Computational Physics* 1992; 100: 143–162. DOI:10.1016/0021-9991(92)90316-Q.

[38] Morris E BT Lusk and Hoffman JM. Influence of street intersections on last channelling diffraction effects. In *Proceedings of the Annual Conferences on Explosives and Blasting Technique*. Nashville, Tennessee, pp. 12–15.

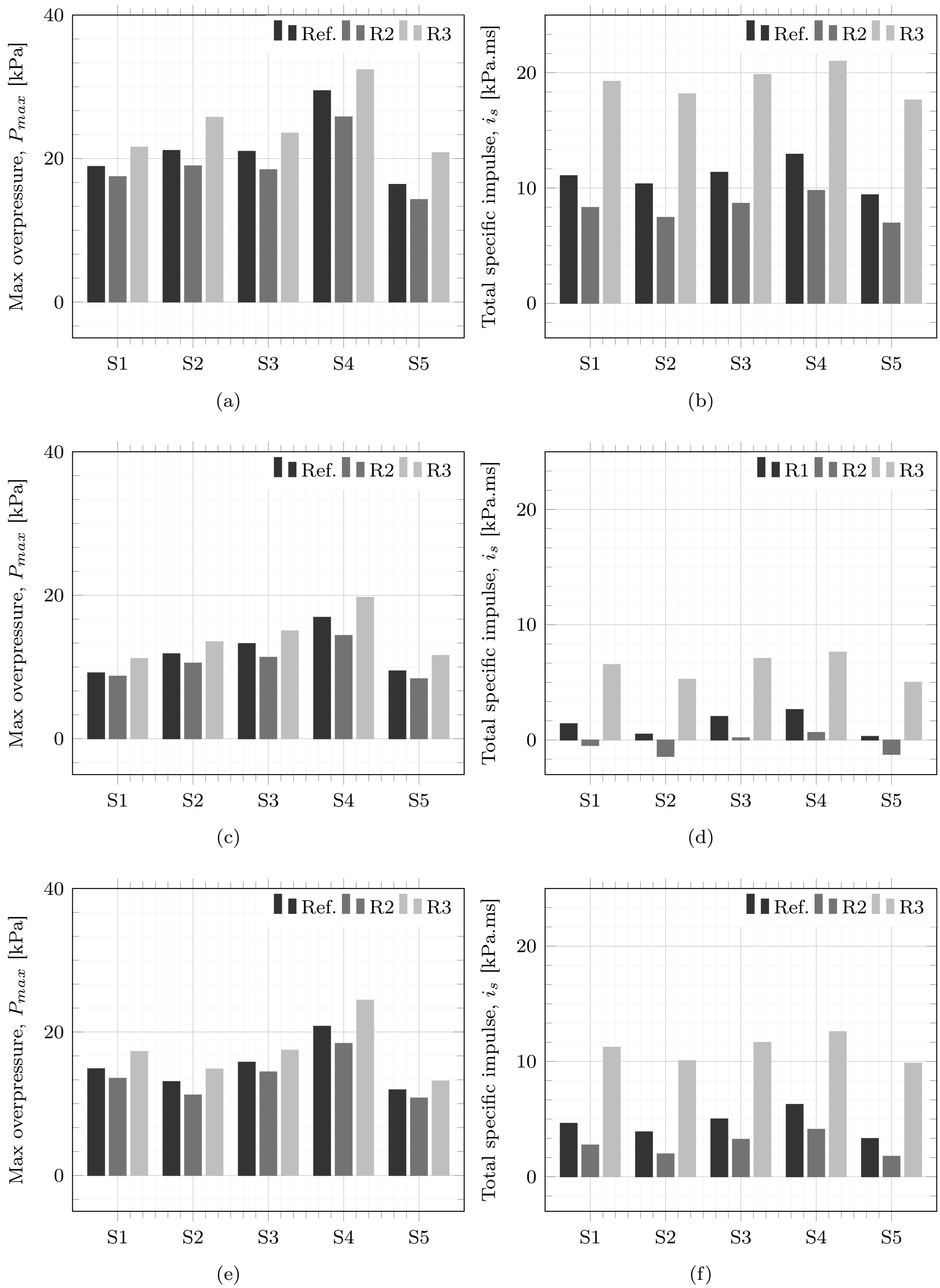

Figure 7. Maximum overpressure and specific impulse for different roof extensions with charges located at (a-b) $45°$, (c-d) $0°$ and (e-f) $90°$.

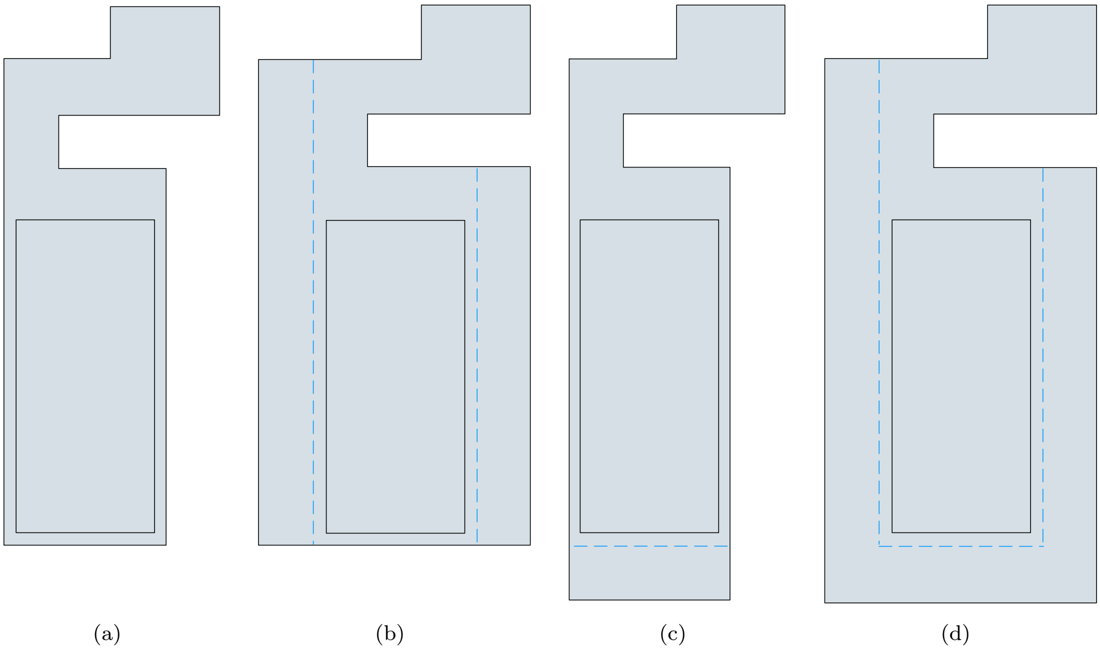

Figure 8. Corridor dimension layouts: (a) Reference, (b) C1, (c) C2 and (d) C3.

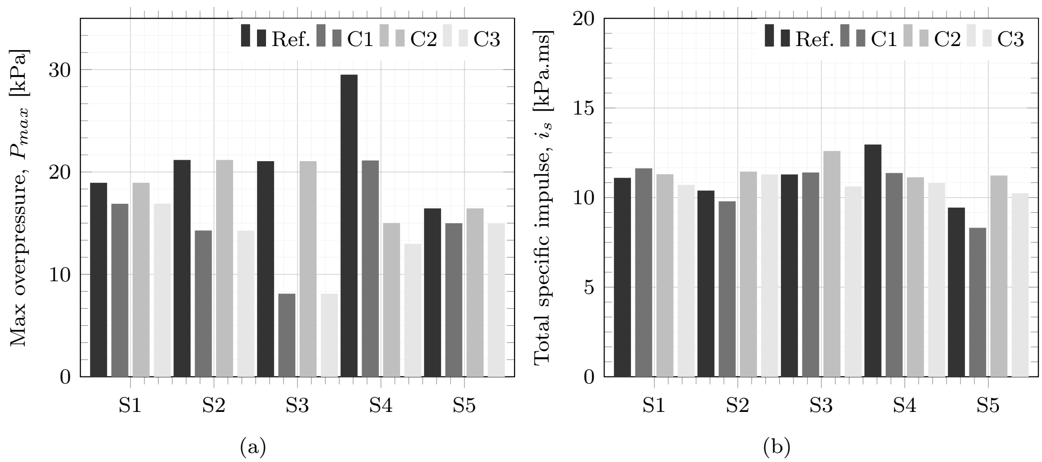

Figure 9. Comparison of (a) maximum overpressure and (b) specific impulse for different corridor widths.

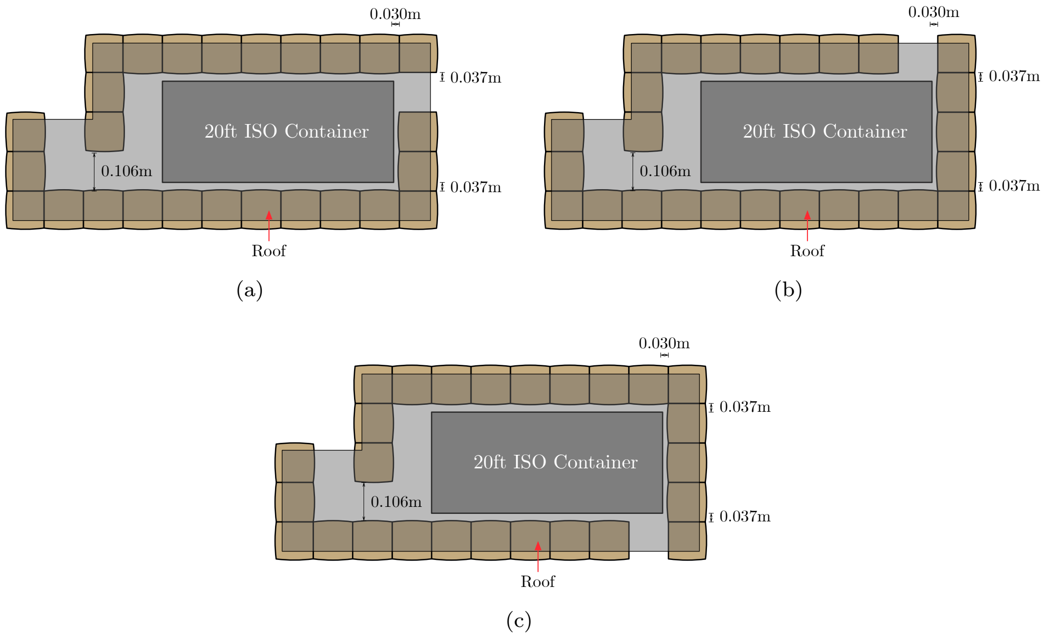

Figure 10. Venting locations on the reference HBC: opening at the (a) rear (BO), (b) left side (LO) and (c) right side (RO).

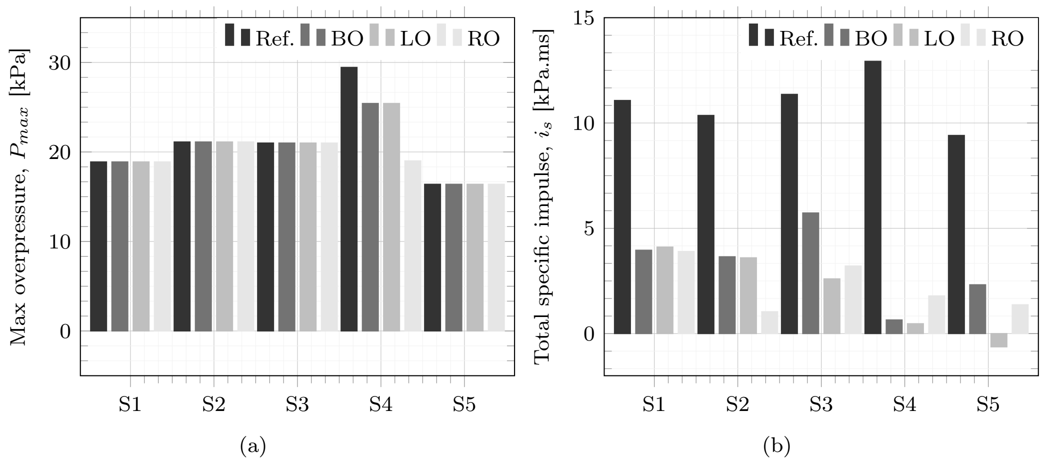

Figure 11. Influence of venting openings on the maximum (a) overpressure and (b) specific impulse.

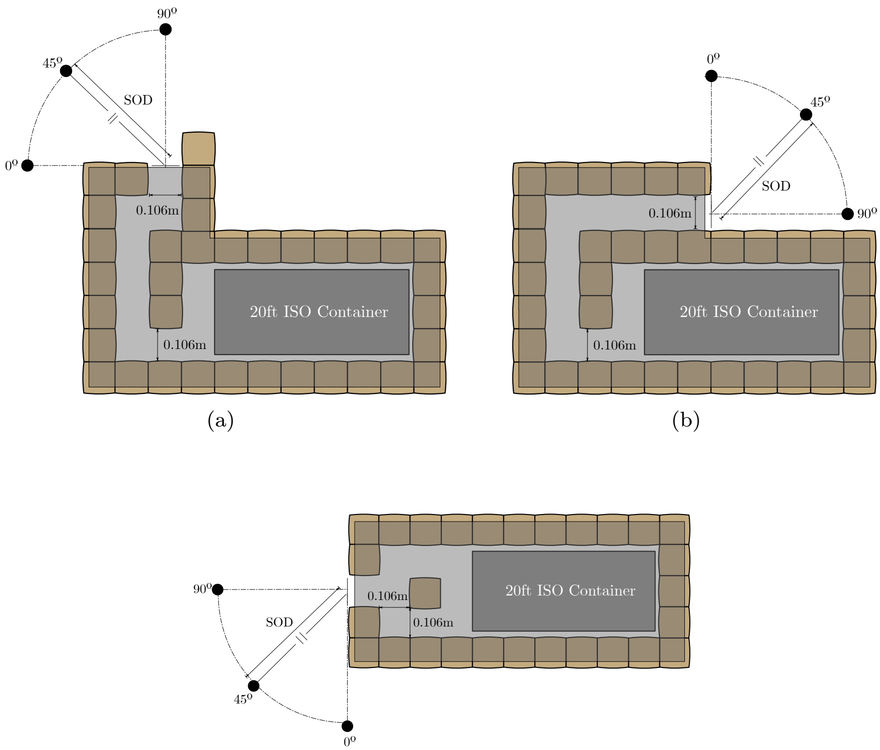

Figure 12. Modified entrance layouts: (a) Entrance 1 (E1), (b) Entrance 2 (E2) and (c) Entrance 3 (E3).

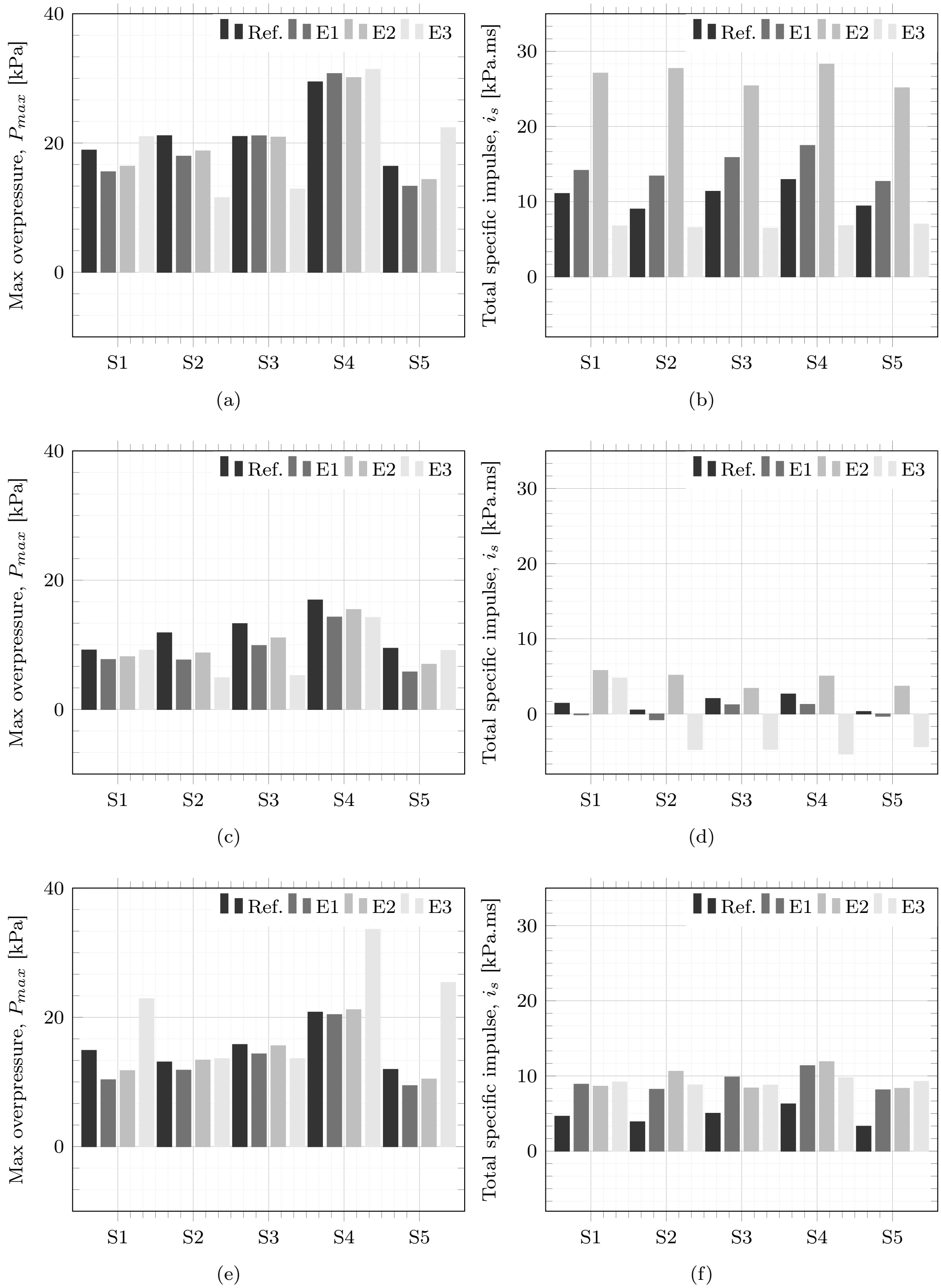

Figure 13. Maximum overpressure and specific impulse for different entrance layouts. The explosive charge is located at a stand-off distance of 1 m and at an angle of incidence of: (a-b) 45°; (c-d) 0° and (e-f) 90°.